ISBN 978-90-481-3408-3

NATO Science for Peace and Security Series - A:
Chemistry and Biology

Metastable Systems under Pressure

Edited by
Sylwester Rzoska
Aleksandra Drozd-Rzoska
Victor Mazur

METASTABLE WATER UNDER PRESSURE

[1]KEVIN STOKELY, [1] MARCO G. MAZZA, [1]H. EUGENE STANLEY, AND[2] GIANCARLO FRANZESE
[1]*Center for Polymer Studies and Department of Physics, Boston University – Boston, MA 02215 USA*
[2]*Departament de Fısica Fonamental – Universitat de Barcelona,Diagonal 647, Barcelona 08028, Spain*

Abstract: We have summarized some of the recent results, including studies for bulk, confined and interfacial water. By analyzing a cell model within a mean field approximation and with Monte Carlo simulations, we have showed that all the scenarios proposed for water's P–T phase diagram may be viewed as special cases of a more general scheme. In particular, our study shows that it is the relationship between H bond strength and H bond cooperativity that governs which scenario is valid. The investigation of the properties of metastable liquid water under pressure could provide essential information that could allow us to understand the mechanisms ruling the anomalous behavior of water. This understanding could, ultimately, lead us to the explanation of the reasons why water is such an essential liquid for life.

Keywords: water, anomalous behavior, simulations

1. Introduction

Water's phase diagram is rich and complex: more than sixtee crystalline phases[1], and two or more glasses[2]. The liquid state also displays intersting behavior. In the stable liquid regime water's thermodynamic response functions behave qualitatively differently than a typical liquid. The isothermal compressibility K_T and isobaric specific heat C_P each display a minimum as a function of temperature (at 46°C and 36°C for 1 atm, respectively) while for a typical liquid these quantities monotonically decrease upon cooling. Water's anomalies become even more pronounced as the system is cooled below the melting point and enters the metastable supercooled regime[3]. Here K_T and C_P increase rapidly upon cooling, with an apparent divergence for 1 atm at −45°C.[4] A precise understanding of the physico–chemical properties of liquid water is important to provide accurate predictions of the behavior of biological molecules[5,6], geophysical structures[7], and

S. Rzoska et al. (eds.), *Metastable Systems under Pressure*,

nanomaterials[8] to mention just a few subjects of interest. Microscopically, the anomalous liquid behavior is understood as resulting from the tendency of water molecules to form hydrogen (H) bonds upon cooling, with a decrease of potential energy, decrease of entropy, and increase of distance between the bonded molecules. The low temperature phase behavior which results from these interactions, however, remains unknown because experiments on bulk water below the crystal homogenous nucleation temperature T_H (−38°C at 1 atm) are unfeasible. Four different scenarios for the pressure–temperature ($P - T$) phase diagram have been debated:

(i) The stability limit (SL) scenario[9] hypothesizes that the superheated liquid spinodal at negative pressure re-enters the positive P region below $T_H(P)$ leading to a divergence of the response functions.
(ii) The singularity–free (SF) scenario[10] hypothesizes that the low-T anticorrelation between volume and entropy gives rise to response functions that increase upon cooling and display maxima at non–zero T, but do not display singular behavior.
(iii) The liquid–liquid critical point (LLCP) scenario[11] hypothesizes a first–order phase transition line with negative slope in the P − T plan, separating a low density liquid (LDL) from a high density liquid (HDL), which terminates at a critical point C′. Below the critical pressure PC′ the response functions increase on approaching the Widom line (the locus of correlation length maxima emanating from C′ into the one–phase region), and for $P > P_{C'}$ by approaching the spinodal line. Evidence suggests[11–13] that $P_{C'} > 0$, but the possibility $P_{C'} < 0$ has been proposed.[14]
(iv) The critical–point free (CPF) scenario[15] hypothesizes a first–order phase transition line separating two liquid phases and extending to $P < 0$ down to the (superheated) limit of stability of liquid water. No critical point is present in this scenario.

Though experiments on bulk water are currently unfeasible, freezing in the temperature range of interest can be avoided for water in confined geometries[16–18] or on the surface of macromolecules.[19–25] Since experiments in the supercooled region are difficult to perform, an intense activity of numerical simulations has been developed in recent years to help interpret of the data[26, 27]. However, simulations at very low temperature T are hampered by the glassy dynamics of the empirical models of water.[28,29] It is therefore important to study simple models, which are able to capture the fundamental physics ofwater while being less computationally expensive. We analyze a microscopic cell model[30] of water that has been shown to exhibit any of the proposed scenarios, depending on choice of parameters.[10,13, 31] The model, whose dynamics behavior compares well with that of supercooled water,[29,32] is here studied using both mean-field (MF) analysis and Monte Carlo (MC) simulations.

2. The cell model

The model consists of dividing the fluid into N cells with index $i \in [1, \ldots, N]$, each with volume v_0, and occupation variable $n_i = 0$ (for a cell with gas–like density) or $n_i = 1$ (for a cell with liquid–like density). Each cell is assumed in contact with 4 nearest neighbor (n.n.) cells, mimicking the first shell of liquid water, in the simplified assumption of no interstitial molecules.

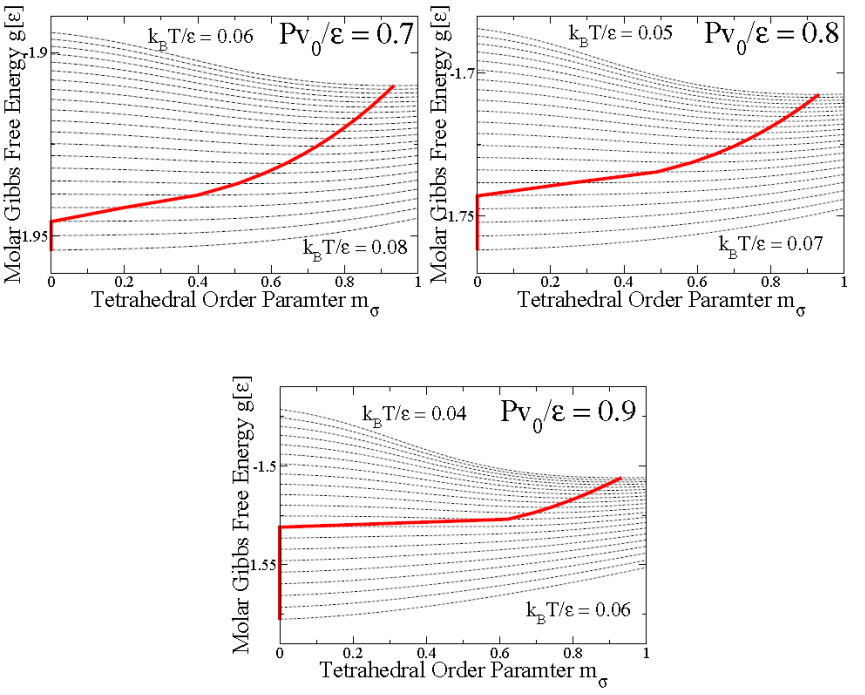

Figure 1. *Numerical minimization of the molar Gibbs free energy g in the mean field approach. The model's parameters are $J/\varepsilon = 0.5$, $J\sigma/\varepsilon = 0.05$, $v_{HB}/v_0 = 0.5$ and $q = 6$. In each panel we present g (dashed lines) calculated at constant P and different values of T. The thick line crossing the dashed lines connects the minima $m_\sigma^{(eq)}$ of g at different T. Upper panel: $Pv_0/\varepsilon = 0.7$, for T going from $k_BT/\varepsilon = 0.06$ (top) to $k_BT/\varepsilon = 0.08$ (bottom). Middle panel: $Pv0/\varrho = 0.8$, for T going from $k_BT/\varepsilon = 0.05$ (top) to $k_BT/\varepsilon = 0.07$ (bottom). Lower panel: $Pv_0/\varepsilon = 0.9$, for T going from $k_BT/\varepsilon = 0.04$ (top) to $k_BT/\varepsilon = 0.06$ (bottom). In each panel dashed lines are separated by $k_B\delta T/\varepsilon = 0.001$. In all the panels $m_\sigma^{(eq)}$ increases when T decreases, being 0 (marking the absence of tetrahedral order) at the higher temperatures and ≈ 0.9 (high tetrahedral order) at the lowest temperature. By changing T, $m_\sigma^{(eq)}$ changes in a continuous way for $Pv_0/\varepsilon = 0.7$ and 0.8, but discontinuous for $Pv_0/\varepsilon = 0.9$ and higher P.*

The system is described by the Hamiltonian [30]:

$$\mathscr{H} = -\epsilon \sum_{\langle i,j \rangle} n_i n_j - J \sum_{\langle i,j \rangle} n_i n_j \delta_{\sigma_{ij},\sigma_{ji}} - J_\sigma \sum_i n_i \sum_{(k,\ell)_i} \delta_{\sigma_{ik},\sigma_{i\ell}}. \quad (1)$$

The first term with $\varepsilon > 0$ accounts for the van der Waals attraction and hard-core volume exclusion, such that neighboring liquid cells are energetically favorable. This term is due to the long–range attraction and short–range repulsion of the electron clouds [33]. The sum is over all n.n. cells h_i, j_i.

The second term with $J > 0$ accounts for the directional H bond interaction between neighboring liquid cells, which must be correctly oriented in order to form a bond.

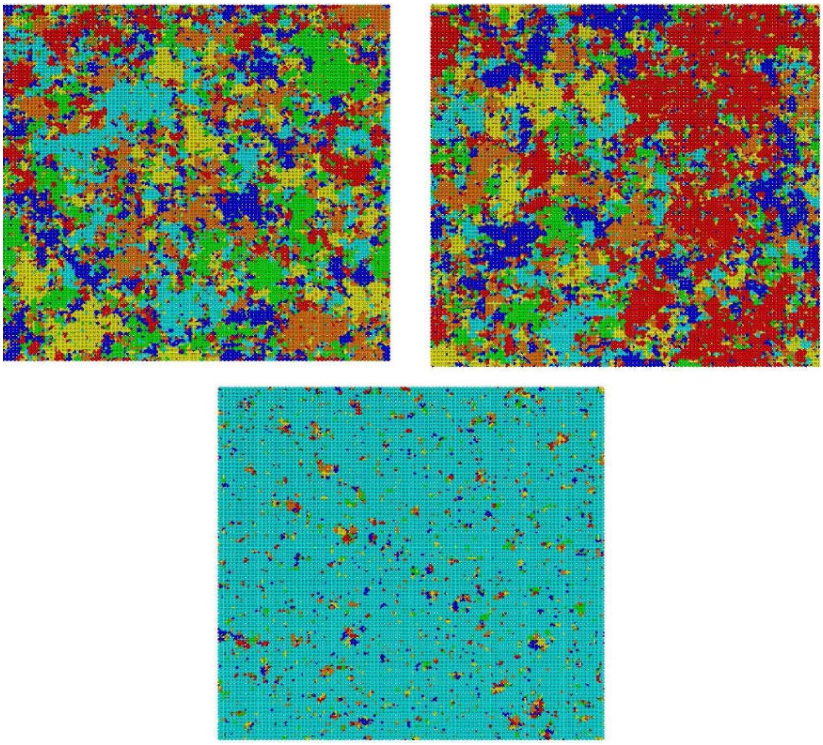

Figure 2. *Three snapshots of the system, for N = 100×100, showing the Wolff's clusters of correlated water molecules. For each molecule we show the states of the four arms and associate different colors to different arm's states. The state points are at pressure close to the critical value P_C ($Pv_0/\varepsilon = 0.72 \approx P_C v_0/\varepsilon$) and $T > T_C$ (top panel, $k_BT/\varepsilon = 0.053$), $T \approx T_C$ (middle panel, $k_BT/\varepsilon = 0.0528$), $T < T_C$ (bottom panel, $k_BT/\varepsilon = 0.052$), showing the onset of the percolation at $T \approx T_C$. At $T \approx T_C$ (middle panel) there is one large cluster, in red on the right, with a linear size comparable to the system linear extension and spanning in the vertical direction.*

This term is associated with the covalent nature of the bond[34]. Bond variables σ_{ij} represent the orientation of the molecules in cell i with respect to the n.n.

molecule in the cell j, and $\delta_{a,b} = 1$ if $a = b$ and $\delta_{a,b} = 0$ otherwise. We choose $q = 6$, giving rise to $6^4 = 1296$ possible orientational states per molecule.

Experiments show that the formation of a H bond leads to a local volume expansion[2], so the total volume is given as

$$V = Nv_0 + N_{HB}v_{HB} \tag{2}$$

$$N_{HB} \equiv \sum_{\langle i,j \rangle} n_i n_j \delta_{\sigma_{ij},\sigma_{ji}} \tag{3}$$

is the total number of H bonds, and v_{HB} is the specific volume increase due to H bond formation.[10] The third term in Eq. (1) with $J_\sigma \geq 0$ represents the many–body interaction among H bonds, related to the T-dependent O–O–O correlation[35], driving the molecules toward a local tetrahedral configuration.[36–39] Here $(k, \ell)_i$ indicates one of the six different pairs of the four bond variables of molecule i. This interaction introduces a cooperative behavior among bonds, which may be fine tuned by changing J_σ. Choosing $J_\sigma = 0$ leads to fully independent H bonds, while $J_\sigma \to \infty$ leads to fully dependent bonds.

3. The mean field analysis

In the MF analysis the macrostate of the system in equilibrium at constant P and T is determined by a minimization of the Gibbs free energy per molecule, $g \equiv \left(\langle \mathcal{H} \rangle - PV + TS\right)/N_w$

$$N_w = \sum_i n_i \tag{4}$$

the total number of liquid-like cells, and $S = S_n + S_\sigma$ is the sum of the entropy Sn over the variables n_i and the entropy S_σ over the variables σ_{ij}. A MF approach consists of writing g explicitly using the approximations

$$\sum_{<ij>} n_i n_j \longrightarrow 2Nn^2 \qquad \sum_{<ij>} n_i n_j \delta_{\sigma_{ij},\sigma_{ji}} \longrightarrow 2Nn^2 p_\sigma$$

$$\sum_i n_i \sum_{(k,l)_i} \delta_{\sigma_{ik},\sigma_{il}} \longrightarrow 6Nnp_\sigma \tag{5-7}$$

where $n = N_w/N$ is the average of n_i, and p_σ is the probability that two adjacent bond indices σ_{ij} are in the same state. Therefore, in this approximation we can write

$$V = Nv_0 + 2Nn^2 p_\sigma v_{HB}$$

$$\langle \mathcal{H} \rangle = -2Nn\left[\epsilon n + (Jn + 3J_\sigma)\, p_\sigma\right] \tag{8,9}$$

The probability p_σ that two adjacent bond variables form a bond is properly defined as the thermodynamic average of $\delta_{\sigma ij\ ,\sigma ji}$ over the entire system. It is here approximated as the average over two neighboring molecules, under the effect of the mean-field h of the surrounding molecules,

$$p_\sigma = \left\langle \delta_{\sigma_{ij},\sigma_{ji}} \right\rangle_h \tag{10}$$

The ground state of the system consists of all N variables $n_i = 1$, and all σ_{ij} in the same state. At low temperatures the symmetry will remain broken, with the majority of the σ_{ij} in a preferred state. We associate this preferred state with the space-filling tetrahedral network of H bonds formed by liquid water, and define n_σ as the density of bond indices in this tetrahedral state, with $1/q \le n_\sigma \le 1$. An appropriate form for h is[30]

$$h = 3J_\sigma \frac{1 + (q-1)m_\sigma}{q} \tag{11}$$

where $0 \le m_\sigma \le 1$ is an order parameter associated with the number of bond variables in the preferred state.

Equating the MF relation

$$p_\sigma \equiv n_\sigma^2 + \frac{(1-n_\sigma)^2}{q-1} \tag{12}$$

with the approximate expression in Eq. (10) allows us to express n_σ in terms of T, P, and m_σ, which may be substituted into the MF expression for g. The MF approximations for the entropies S_n of the N variables n_i, and S_σ of the $4Nn$ variables σ_{ij}, are[40]

$$S_n = -k_B N(n\log(n) + (1-n)\log(1-n)) \tag{13,14}$$
$$S_\sigma = -k_B 4Nn[n_\sigma \log(n_\sigma) + (1-n_\sigma)\log(1-n_\sigma) + \log(q-1)]$$

where k_B is the Boltzmann constant.

Minimizing numerically g with respect to n and m_σ, we find the equilibrium values $n^{(eq)}$ and $m_\sigma^{(eq)}$. By substitution into Eqs. (4) and (2), we calculate the density ρ at any (T, P), the full equation of state. An example of the minimization of g is presented in Fig. 1 where, for the model parameters $J/\varepsilon = 0.5$, $J_\sigma/\varepsilon = 0.05$, $v_{HB}/v_0 = 0.5$ and $q = 6$, a discontinuity in $m_\sigma^{(eq)}$ is observed for $Pv_0/\varepsilon > 0.8$. As discussed in Refs. [13, 30] this discontinuity corresponds to a first order phase transition between two liquid phases with different degree of tetrahedral order and, as a consequence, different density. The P at which the change in $m_\sigma^{(eq)}$ becomes continuous corresponds to the pressure of a LLCP. The occurrence of the LLCP is consistent with one of the possible interpretations of the anomalies of water, as discussed in Ref. [40]. However, for different choices of parameters, the model reproduces also the other proposed scenarios.[31]

4. The Monte Carlo simulations

To perform MC simulations in the NPT ensemble, we consider a modified version of the model in which we allow for continuous volume fluctuations. To this goal, (i) we assume that the system is homogeneous with all the variables n_i set to 1 and all cells have volume $v = V/N$; (ii) we consider that $V \equiv V_{MC} + N_{HB}v_{HB}$, where $V_{MC} > N_{v0}$ is a dynamical variable allowed to fluctuate in the simulations; (iii) we replace the first (van der Waals) term of the Hamiltonian in Eq. (1) with a Lennard-Jones potential with attractive energy $\varepsilon > J$ plus a hard-core interaction

$$U_W(r) \equiv \begin{cases} \infty & \text{if } r \leqslant r_0, \\ \epsilon\left[\left(\frac{r_0}{r}\right)^{12} - \left(\frac{r_0}{r}\right)^{6}\right] & \text{if } r > r_0. \end{cases} \tag{15}$$

where $r_0 \equiv (v_0)^{1/d}$;[13] the distance between two n.n. molecules is $(V/N)^{1/d}$, and the distance r between two generic molecules is the Cartesian distance between the center of the cells in which they are included. The simplification (i) could be removed, allowing the cells to assume different volumes v_i and keeping fixed the number of possible n.n. cells. However, results of the model under the simplification (i) compare well with experiments.[40] Furthermore, the simplification (i) allows to drastically reduce the computational cost of the evaluation of the $U_{W(r)}$ term from $N(N-1)$ to $N-1$ operations.

MC simulations are performed with $N = 10^4$ molecules, each with four n.n. molecules on a 2d square lattice, at constant P and T, and with the same model parameters as for the MF analysis. To each molecules we associate a cell on a square lattice. The Wolff's algorithm is based on the definition of a cluster of variables chosen in such a way to be thermodynamically correlated.[41, 42] To define the Wolff's cluster, a bond index (arm) of a molecule is randomly selected; this is the initial element of a stack. The cluster is grown by first checking the remaining arms of the same initial molecule: if they are in the same Potts state, then they are added to the stack with *probability* $p_{same} \equiv min\,[1,\ 1 - exp(-\beta J_\sigma)]$,[43] where $\beta \equiv (k_B T)^{-1}$. This choice for the probability p_{same} depends on the interaction J_σ between two arms on the same molecule and guarantees that the connected arms are thermodynamically correlated. [41] Next, the arm of a new molecule, facing the initially chosen arm, is considered. To guarantee that connected facing arms correspond to thermodynamically correlated variables, is necessary[42] to link them with the probability $p_{facing} \equiv min\,[1,\ 1 - exp(-\beta J')]$ where $J' \equiv J - P v_{HB}$ is the P–dependent effective coupling between two facing arms as results from the enthalpy H +PV of the system. It is important to note that J' can be positive or negative

depending on P. If $J' > 0$ and the two facing arms are in the same state, then the new arm is added to the stack with probability p_{facing}; if $J' < 0$ and the two facing arms are in different states, then the new arm is added with probability p_{facing}.[44] Only after every possible direction of growth for the cluster has been considered the values of the arms are changed in a stochastic way; again we need to consider two cases: (i) if $J' > 0$, all arms are set to the same new value

$$\sigma^{\text{new}} = \left(\sigma^{\text{old}} + \phi\right) \mod q \tag{16}$$

where φ is a random number between 1 and q; (ii) if $J' < 0$, the state of every single arm is changed (rotated) by the same random constant $\varphi \in [1, \ldots q]$

$$\sigma_i^{\text{new}} = \left(\sigma_i^{\text{old}} + \phi\right) \mod q. \tag{17}$$

In order to implement a constant P ensemble we let the volume fluctuate. A small increment $\Delta r/r_0 = 0.01$ is chosen with uniform random probability and added to the current radius of a cell. The change in volume $\Delta V \equiv V^{new} - V^{old}$ and van der Waals energy ΔE_W is computed and the move is accepted with probability $min\,(1, exp\,[-\beta\,(\Delta E_W + P\Delta V - T\Delta S)])$, where $\Delta S \equiv -Nk_B ln(V^{new}/V^{old})$ is the entropic contribution. The cluster MC algorithm turns out to be hundreds of time faster, in generating uncorrelated configurations, than a Metropolics MC dynamics when the system has P and T in the vicinity of the liquid critical point. The efficiency of the Wolff's cluster algorithm is a consequence of the exact relation between the average size of the finite clusters and the average the size of the regions of thermodynamically correlated molecules. The proof of this relation at any T derives straightforward from the proof for the case of Potts variables[41] This relation allows to identify the clusters built during the MC dynamics with the correlated regions and emphasizes (i) the appearance of heterogeneities in the sturctural correlations,[45] and (ii) the onset of percolation of the clusters of tetrahedrally ordered molecules at the liquid–liquid critical point,[46] as shown in Fig. 2.

5. Effects of the hydrogen bond strength and cooperativity

From the MF analysis, when $J_\sigma = 0$ the model coincides with the one proposed in[10] which gives rise to the SF scenario (Fig. 3a). When $J_\sigma > 0$ the model displays a phase diagram with a LLCP (Fig. 3b) [13]. For $J_\sigma \to 0$, keeping J and the other parameters constant, we find that $T_{C'} \to 0$, and the power–law behavior of K_T and the isobaric thermal expansion coefficient α_P is preserved. Further, we find for the entropy S that, for any value of J_σ, $(\partial S/\partial T)_P \sim |T - T_{C'}|^{-1}$.

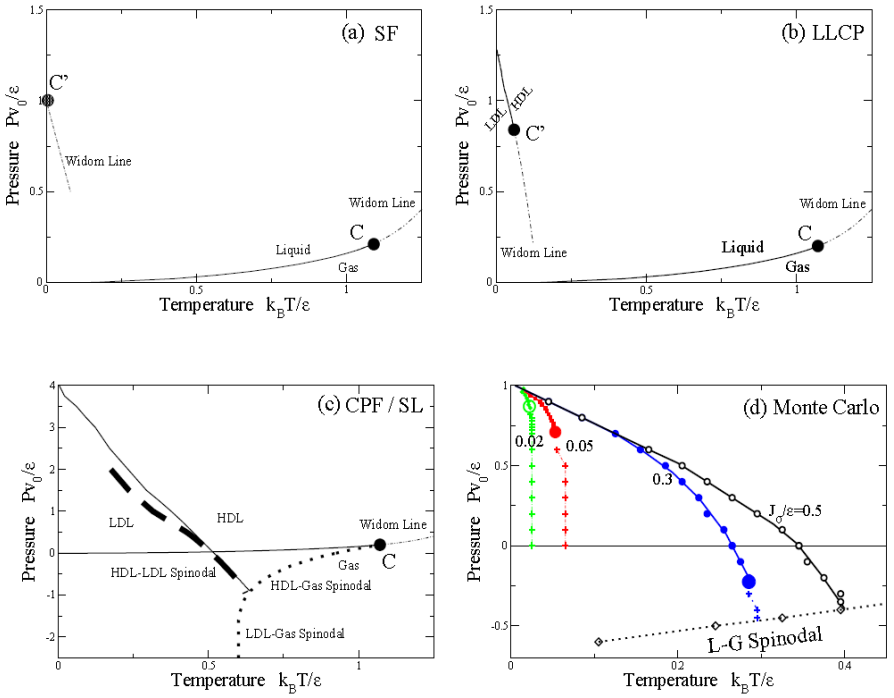

Figure 3. *Phase diagram predicted from our calculations for the cell model with fixed H bond strength ($J/\varepsilon = 0.5$), fixed H bond volume increase ($v_{HB}/v_0 = 0.5$), and different values of the H bond cooperativity strength J_σ. (a) Singularity-free scenario ($J_\sigma = 0$) from MF calculations. At high T, liquid (L) and gas (G) phases are separated by a first order transition line (thick line)ending at a critical point C, from which a L–G Widom line (double–dot–dashed line) emanates. In the liquid phase, the α_P maxima and the K_T maxima increase along lines that converge to a locus (dot–dashed line). In C' both α_P and K_T have diverging maxima. The locus of the maxima is related to the L-L Widom line for $T_{C'} \rightarrow 0$ (see text). (b) Liquid–liquid critical point scenario (for$J_\sigma/\varepsilon = 0.05$) from MF calculations. At low T and high P, a high density liquid (HDL) and a low density liquid (LDL) are separated by a first order transition line (thick line) ending in a critica lpoint C', from which the L-L Widom line emanates. Other symbols are as in the previous panel.(c) Critical–point free scenario ($J_\sigma/\varepsilon = 0.5$) from MF calculations. The HDL–LDL coexistence line extends to the superheated liquid region at $P < 0$, merging with the liquid spinodal (dotted line) hat bends toward negative P. The stability limit (SL) of water at ambient conditions (HDL) is limited by the superheated liquid–to–gas spinodal and the supercooled HDL–to–LDL spinodal (long–dashed thick line), giving a re-entrant behavior as hypothesized in the SL scenario. Other symbols are as in the previous panels. (d) Phase diagram from MC simulations, for $J_\sigma/\varepsilon = 0.02, 0.05, 0.3, 0.5$ (thick lines with symbols and labels). For $J_\sigma/\varepsilon = 0.5$, we find the CPF scenario, as in panel (c). For $J_\sigma/\varepsilon = 0.3$, we find C' (large circle) at $P < 0$ [14], with the L-L Widom line (crosses). For $J_\sigma/\varepsilon = 0.05$, we find the LLCP scenario with C' at $P > 0$, as in panel (b). For $J_\sigma/\varepsilon = 0.02$, C' approaches $T = 0$ as in the SF scenario in panel (a). Errors are of the order of the symbol sizes. Lines are guides for the eyes. In all panels, k_B is the Boltzmann constant.*

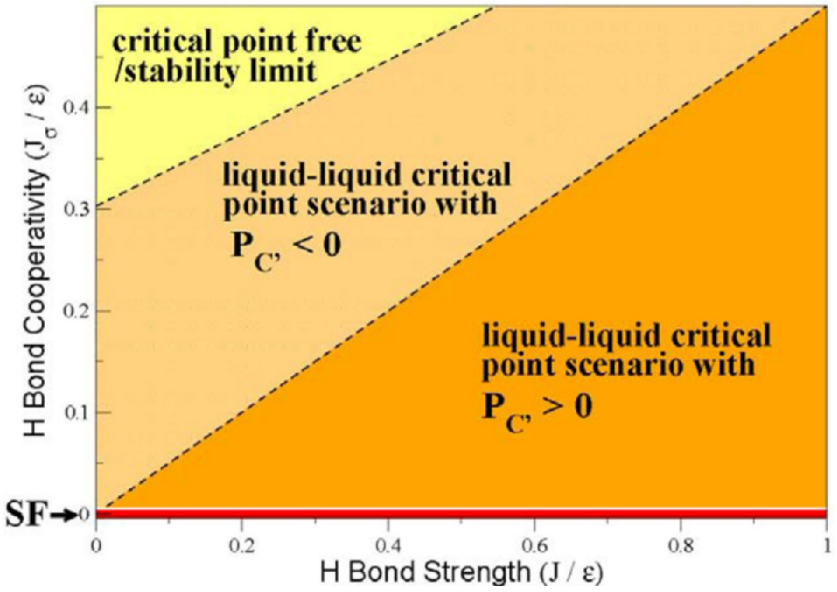

Figure 4. *Possible scenarios for water for different values of J, the H bond strength, and J_σ, the strength of the cooperative interaction, both in units of the van der Waals energy ε. The ratio v_{HB}/v_0 is kept constant. (i) If $J_\sigma = 0$ (red line), water would display the singularity free (SF) scenario, independent of J. (ii) For large enough J_σ, water would possess a first–order liquid–liquid phase transition line terminating at the liquid–gas spinodal—the critical point free (CPF) scenario; the liquid spinodal would retrace at negative pressure, as in the stability limit (SL) scenario (yellow region). (iii) For other combinations of J and J_σ, water would be described by the liquid–liquid critical point (LLCP) scenario. For large J_σ, the LLCP is at negative pressure (ochre region). For small J_σ, the LLCP is at positive pressure (orange region). Dashed lines separating the three different regions correspond to mean field results of the microscopic cell model. The P − T phase diagram evolves continuously as J and J_σ change.*

This critical behavior of the derivative of S implies that $C_P \equiv T(\partial S/\partial T)_P$ diverges when is non–zero ($J_\sigma > 0$), but C_P is constant for the case $T_{C'} = 0$ ($J_\sigma = 0$), which corresponds to the SF scenario.[10] Therefore, the SF scenario coincides with the LLCP scenario in the limiting case of $T_{C'} \to 0$ for $J_\sigma \to 0$ (Fig. 4). Next, we increase J_σ/J, keeping J constant, and observe that C' moves to larger T and lower P. For $J_\sigma > J/2$, we observe that $P_{C'} < 0$ as in.[14] By further increasing J_σ, we observe that the liquid–liquid coexistence line intersects the liquid–gas spinodal, which is precisely the CPF scenario (Fig. 3c).[15,47] As in Ref. [12], we find that the superheated liquid spinodal merges with the supercooled liquid spinodal, giving rise to a retracing spinodal as in the SL scenario. Hence, the CPF scenario and the SL scenario (i) coincide and (ii) correspond to the case in which the cooperative behavior is very strong. In

Fig 4. we summarize our results in the J/ε vs. J_σ/ε parameter space. The MC simulations confirm the MF results (Fig. 3d). For large values of J_σ ($J_\sigma = J = 0.5\varepsilon$), we find a HDL–LDL first–order phase transition that merges with the superheated liquid spinodal as in the CPF scenario. At lower Jσ ($J_\sigma = 0.6J = 0.3\varepsilon$), a HDL–LDL critical point appears at $P < 0$,[14] with the liquid–liquid Widom line intersecting the superheated liquid spinodal. By further decreasing J_σ ($J_\sigma = J/10 = \varepsilon/20$), the HDL–LDL critical point occurs at $P > 0$ as in the LLCP scenario, with the liquid–liquid Widom line intersecting the $P = 0$ axis. By approaching $J_\sigma = 0$ ($J_\sigma = J/25 = \varepsilon/50$), we find that the temperature of the HDL–LDL critical point approaches zero and the critical pressure increases toward the value $P = \varepsilon/v_0$ independent of J_σ. The liquid–liquid Widom line approaches the $T = 0$ axis, consistent with our MF results for $\mathbf{J_\sigma \rightarrow 0}$. Thus, we offer a relation linking the four proposed scenarios, showing that (i) all can be included in one general scheme and (ii) the balance between the energies of two components of the H bond interaction determines which scenario is valid.

6. Changes with pressure of the specific heat

Our MF calculations and MC simulations of the cell model allow us to offer also an intringuing interpretation[51] of a phenomenon recently observed. Recent experiments on water confined in cylindrical silica gel pores with diameters of 1.2–1.8 nanometers allow to probe extremely low temperatures that are inaccessible to bulk water. Under these conditions, two maxima in C_P have been observed as the temperature decreases.[48–50] A prominent peak at low T is accompanied by a smaller and broader peak at higher T. These experiments have been interpreted in terms of non-equilibrium dynamics [50]. Our analysis, instead, provides a thermodynamic interpretation, supported by very recent experiments .[52, 53] From simulations for the model parameters J/ε = 0.5, $J_\sigma/\varepsilon = 0.05$, $v_{HB}/v_0 = 0.5$ and $q = 6$, we calculate $C_P \equiv (\partial H/\partial T)_P$, where $H = \langle E \rangle + P\langle V \rangle$ is the enthalpy, and $\langle\ \rangle$ denotes the thermodynamic average. For low pressure isobars, such as $P_{v0}/\varepsilon = 0.001$, we observe the presence of two C_P maxima: one, at higher T, and the second, at lower T, sharper [Fig. 5(a)]. The less sharp maximum moves to lower T and eventually merges with the sharper maximum as P is raised toward P_c. The temperature of the sharper maximum does not change much with P at low P; its value slowly increases, reaching the largest values at the critical pressure P_c .[54] Approaching P_c from below the two maxima merge. For $P > P_c$ this maximum occurs at the temperature of the first-order liquid-liquid (LL) phase transition. For $P >> P_c$ the two maxima split: C_P for the sharper maximum decreases in value and shifts to lower T along the LL

phase transition line, while C_P for the less sharp maximum is independent of P [Fig. 5(b)], as has been noted.[55, 56]

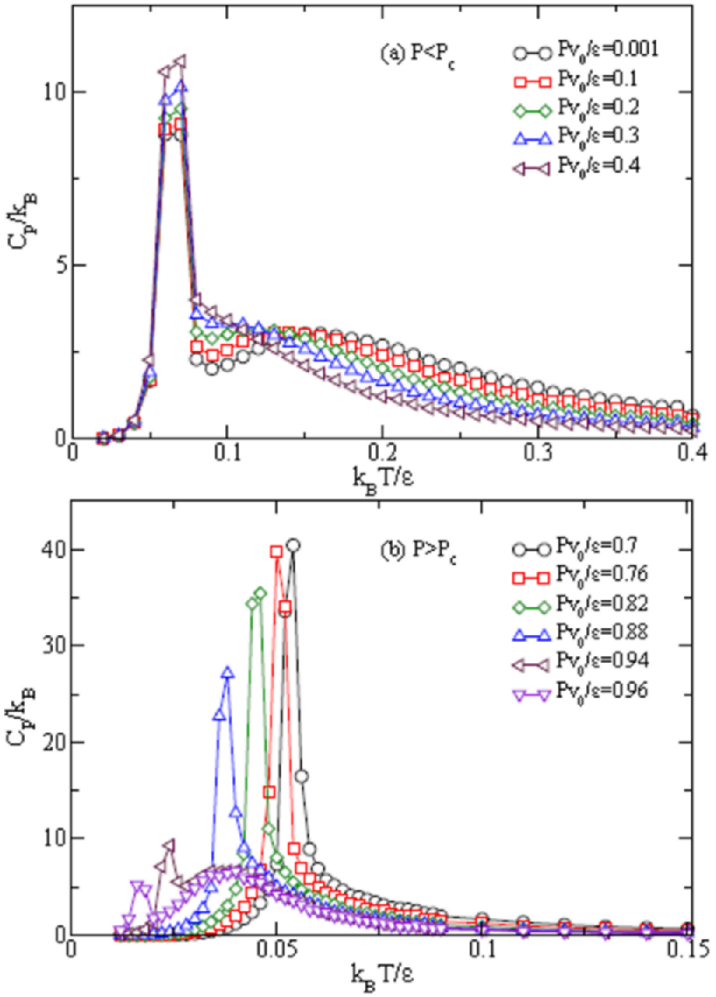

Figure 5. *(a) Temperature dependence of the specific heat CP from MC simulations, for the parameters in the text, along low pressure isobars with $P < P_C$. A broad maximum is visible along with a more pronounced one at lower T. The first maximum moves to lower T as the pressure is raised and it merges with the low–T maximum at $Pv/\varepsilon \approx 0.4$. Upon approaching $P_C v_0/\varepsilon = 0.70 \pm 0.02$ the sharp maximum increases in value. (b) Same for $P \geq P_C$: the two maxima are separated only for $Pv_0/\varepsilon > 0.88$; the sharp maximum decreases as P increases. In both panels errors are smaller han symbol size.*

We also calculate C_P in the MF approximation.[40] We find that the two maxima are distinct only well below P_c [Fig. 6(a)]. Both maxima move to lower T as P increases, though the less sharp maximum at higher T has a more pronounced

P–dependence. Above $P_{v0}/$ 0.3, the two maxima merge into a single maximum.

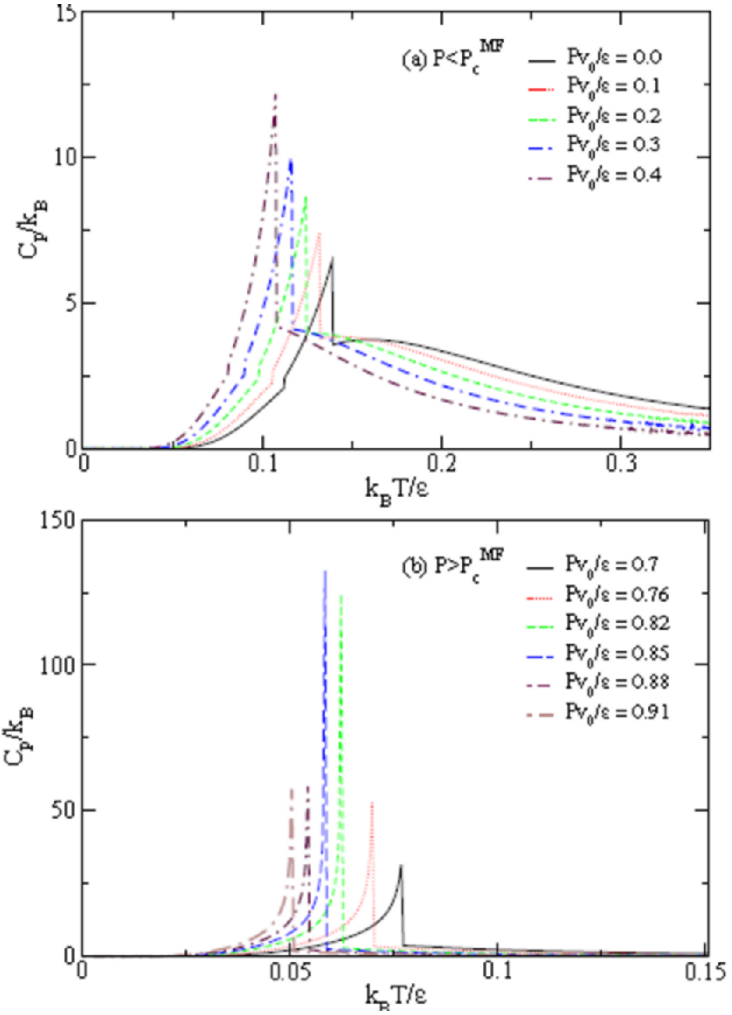

Figure 6. *Same as in Fig. 5 but from mean-field calculations (a) at P<PMFc and (b) at P > P_c^{MF}. The mean-field critical pressure is = 0.81 0.04.*

We also find that for higher P [Fig. 6(b)] the maximum of C_P increases on approaching the MF critical pressure $P_c^{MF}v_0/ = 0.81\pm0.04$ and that the single maximum for $P > P_c^{MF}$ marks the LL phase transition line.[54, 57]

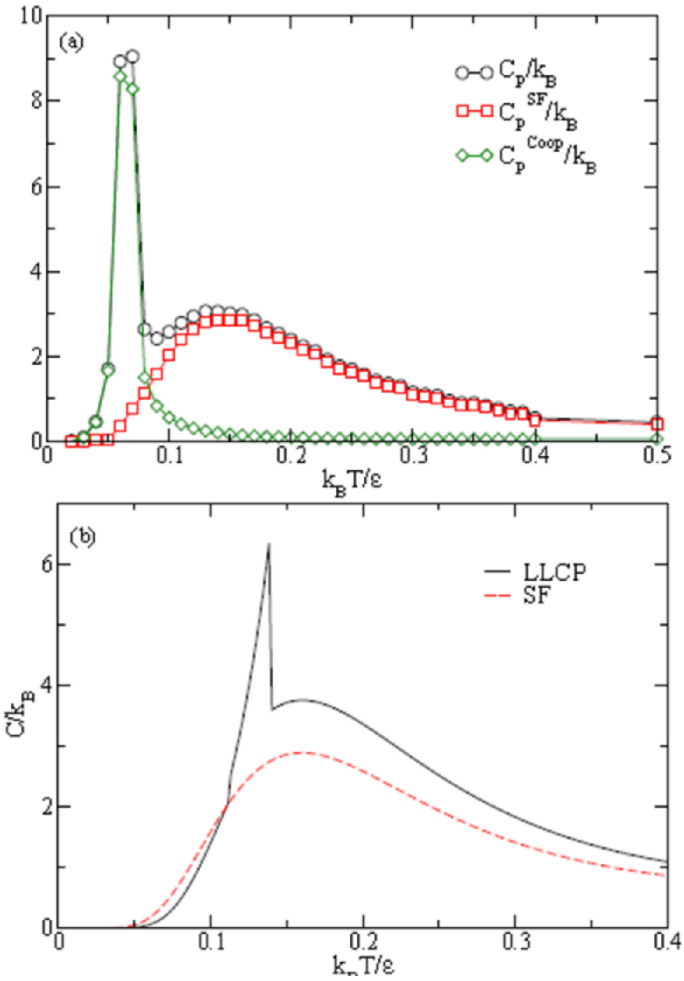

Figure 7. *(a) Decomposition of C_P from MC simulations [Fig. 5] for $Pv0/\varepsilon = 0.1$ into the cooperative component C_P^{Coop} and the SF component C_P^{SF}. (b) Comparison of MF calculations for the LLCP scenario case ($J_\sigma/\varepsilon = 0.05$) and the SF case ($J_\sigma = 0$). The low-T maximum is present only in the LLCP case. Both lines are calculated at $Pv_0/\varepsilon = 0.1$.*

To understand the origin of the two C_P maxima, we write the enthalpy as the sum of two terms

$$H = H^{SF} + H^{Coop} \tag{18}$$

where $H^{SF} \equiv \langle -JN_{HB} + P(V_{MC} + NH_{B\nu HB})\rangle$ and $H_{Coop} \equiv H - H^{SF}$. Hence, we consider $C_P = C_P^{SF} + C_p^{Coop}$, where we define the SF component $C_P^{SF} \equiv (\partial H^{SF}/\partial T)_P$ and the cooperative component $C_P^{Coop} \equiv \partial H^{Coop}/\partial T)_P$ [Fig. 7(a)].

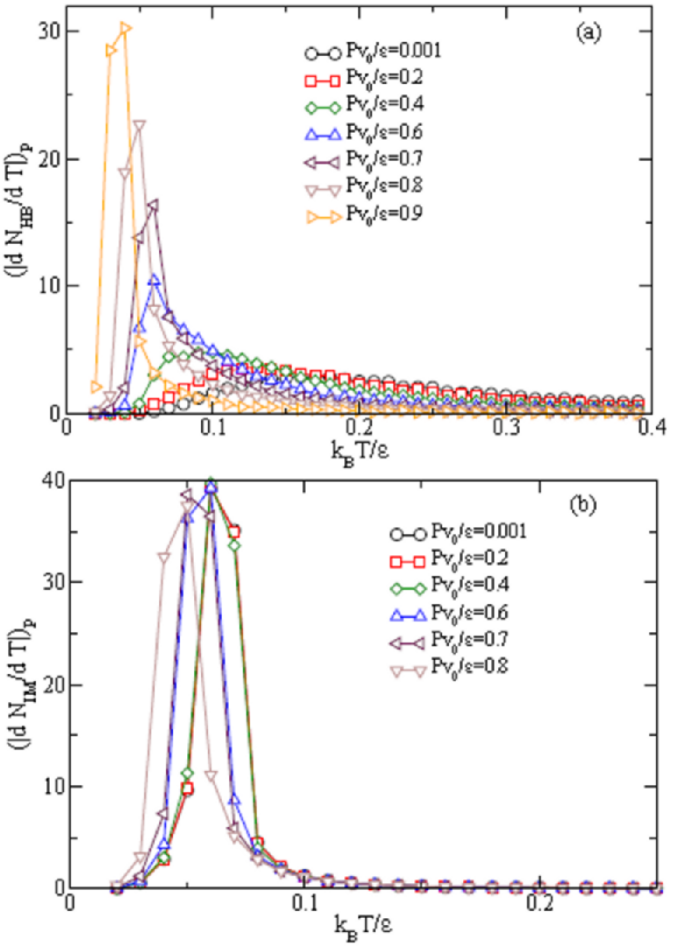

Figure 8. *(a) Temperature dependence of* $(|dN_{HB}/dT|)_P$ *for different isobars. (b) Temperature dependence of* $(|dN_{IN}/dT|)_P$ *for different isobars.*

C^P_{SF} is responsible for the broad maximum at higher T. C_P^{SF} captures the enthalpy fluctuations due to the hydrogen bond formation given by the terms proportional to the hydrogen bond number N_{HB}. This term is present also in the SF model[10]. To show that this maximum is due to the fluctuations of hydrogen bond formation, we calculate the locus of maximum fluctuation of N_{HB}, related to the maximum of $|dN_{HB}/dT|_P$ [Fig. 8(a)], and find that the temperatures of these maxima correlate very well with the locus of maxima of C_P^{SF} [Fig. 9].We

find in Fig. 7(a) that the maximum of C_P at lower T is given by the maximum of C_P^{Coop}. To show that C_P^{Coop} corresponds to the enthalpy fluctuations due to the IM term in Eq. 1 proportional to J_σ,[58] we calculate $|dN_{IM}/dT|_P$, where N_{IM} is the number of molecules with complete tetrahedral order. We find that the locus of maxima of $|dN_{IM}/dT|_P$ [Fig. 8(b)] overlaps with the locus of maxima of C_P^{Coop} [Fig. 9].

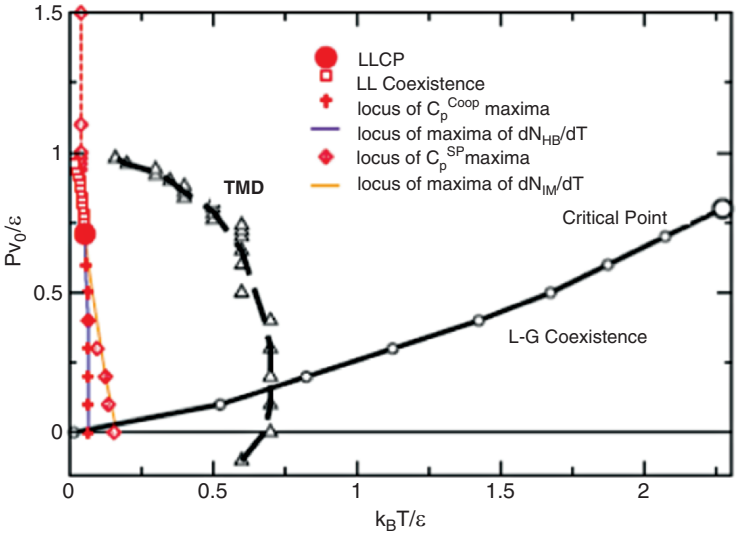

Figure 9. *Phase diagram from MC simulations showing the liquid–gas transition (thick line), the liquid–liquid transition (squares) and the temperature of maximum density (TMD). Emanating from the LLCP (full circle) is the locus of maxima of C_P^{Coop} (crosses), the locus of maxima of C_P^{SF} (diamonds), the locus of maxima of $|dN_{HB}/dT|$ (dark line) and the locus of maxima of $|dN_{IM}/dT|$ (light line). At pressure above the LLCP, a dashed line connects as a guide for the eyes the locus of maxima of C_P^{SF}.*

Therefore, the maximum of C_P^{Coop} occurs where the correlation length associated with the tetrahedral order is maximum, i.e. along the Widom line associated with the LL phase transition.[40] In MF we may compare C_P calculated for the LLCP scenario ($J_\sigma > 0$) with C_P calculated for the SF scenario ($J_\sigma = 0$) [Fig. 7(b)]. We see that the sharper maximum is present only in the LLCP scenario, while the less sharp maximum occurs at the same T in both scenarios. We conclude that the sharper maximum is due to the fluctuations of the tetrahedral order, critical at the LLCP, while the less sharp maximum is due to fluctuations in bond formation. The similarity of our results with the experiments in nanopores is striking.[50] Data in ref. [50] show two maxima in C_P. They have been interpreted as an out–of–equilibrium dynamic effect in [15,50], but more recent experiments [52,53] show that they are a feature of equilibrated confined water. Therefore, our interpretation of the two maxima is of considerable interest.

7. Conclusion

The behavior of metastable water under pressure is the object of an intense experimental and theoretical investigation. Here we have summarized some of the recent results, including studies for bulk, confined and interfacial water. By analyzing a cell model within a mean field approximation and with Monte Carlo simulations, we have showed that all the scenarios proposed for water's P–T phase diagram may be viewed as special cases of a more general scheme. In particular, our study shows that it is the relationship between H bond strength and H bond cooperativity that governs which scenario is valid. We have also considered recent experiments on confined water at low temperatures that display two maxima in the specific heat. Our analysis of metastable water at very low T and for increasing P, provides an intriguing interpretation of the phenomenon, based exclusively on the thermodynamic properties of water. In conclusion, the investigation of the properties of metastable liquid water under pressure could provide essential information that could allow us to understand the mechanisms ruling the anomalous behavior of water. This understanding could, ultimately, lead us to the explanation of the reasons why water is such an essential liquid for life.

References

1. Zheligovskaya, E. A., and Malenkov, G. G. (2006) *Russ. Chem. Rev.* **75**, 57
2. Debenedetti, P. G., (2003) *J. Phys.: Condens. Matter* **15**, R1669
3. Debenedetti, P. G. and Stanley, H. E. (2003) The Physics of Supercooled and Glassy Water, *Physics Today* **56**, 40
4. Angell, C. A. (1982) in: *Water: A Comprehensive Treatise* vol. 7, edited by F. Franks (Plenum, NewYork)
5. Ball, P. (2008) *Chem. Rev.* **108**, 74
6. Franzese, G., and Rubi, eds. M. (2008) *Aspects of Physical Biology: Biological Water, Protein Solutions, Transport and Replication*, (Springer, Berlin)
7. Anisimov, M. A., Sengers, J. V., and Levelt-Sengers, J. M. H. (2004) in *Aqueous System at Elevated Temperatures and Pressures: Physical Chemistry in Water, Stream and Hydrothmaler Solutions*, edited by D.A. Palmer, R. Fernandez-Prini, A. H. Harvey (Elsevier, Amsterdam)
8. Granick and S., and Bae, S. C. (2008) *Science* **322**, 1477
9. Speedy, R. J. (1982) *J. Phys. Chem.* **86**, 3002
10. Sastry, S., Debenedetti, P. G., Sciortino, F., and Stanley, H. E. (1996) *Phys. Rev. E* **53**, 6144

11. Poole, P. H., Sciortino, F., Essmann, U., and Stanley, H. E. (1992) *Nature* **360**, 324
12. Poole, P. H., Sciortino, F., Grande, T., Stanley, H. E., and Angell, C. A. (1994) *Phys. Rev. Lett*. **73**, 1632
13. Franzese, G., Marques, M., and Stanley, H. E. (2003) *Phys. Rev. E.* **67**, 011103
14. Tanaka, H. (1996) *Nature* **380**, 328
15. Angell, C. A. (2008) *Science* **319**, 582
16. Faraone, A., Liu, L., Mou, C. Y., Yen, C. W., and Chen, S. H. (2004) *J. Chem. Phys.* **121**, 10843
17. Liu, L., Chen, S. H., Faraone, A., Yen, C. W., and Mou, C. Y. (2005) *Phys. Rev. Lett.* **95**, 117802
18. Mallamace, F., Broccio, M., Corsaro, C., Faraone, A., Wanderlingh, U., Liu, L., Mou, C. Y., and Chen, S. H. (2006) *J. Chem. Phys.* **124**, 161102
19. Chen, S.-H., Liu, L., Fratini, E., Baglioni, P., Faraone, A., and Mamontov, E. (2006) *Proc. Natl. Acad. Sci.* USA **103**, 9012
20. Mamontov, E. (2005) *J. Chem. Phys.* **123**, 171101
21. Jansson, H., Howells, W. S., and Swenson, J. (2006) *J. Phys. Chem. B* **110**, 13786
22. Chen, S.-H. et al., (2006) J. Chem. Phys. **125**, 171103
23. Chu, X., Fratini, E., Baglioni, P., Faraone, A., and Chen, S.-H. (2008) *Phys. Rev. E* **77**, 011908
24. Franzese, G., Stokely, K., Chu, X.-Q., Kumar, P., Mazza, M. G., Chen. S.-H., and Stanley, H. E. (2008) *J. Phys.: Cond. Matt.* **20**, 494210
25. Stanley, H. E., Kumar, P., Franzese, G., Xu, L. M., Yan, Z. Y., Mazza, M.G., Chen, S.-H., Mallamace, F., Buldyrev, S. V. (2008) "Liquid polyamorphism: Some unsolved puzzles of water in bulk, nano-confined, and biological environments", in Complex Systems, M. Tokuyama, I. Oppenheim, H. Nishiyama, H, eds. *AIP Conference Proceedings*, **982**, 251
26. Xu, L., Kumar, P., Buldyrev, S. V., Chen, S.-H., Poole, P. H., Sciortino, F., and Stanley, H. E. (2005) *Proc. Natl. Acad. Sci.* **102**, 16558
27. Kumar, P., Yan, Z., Xu, L., Mazza, M. G., Buldyrev, S. V., Chen. S.-H., Sastry, S., and Stanley, H. E. (2006) Phys. Rev. Lett. **97**, 177802
28. Stanley, H. E., Buldyrev, S. V., Franzese, G., Giovambattista, N. F., Starr, W. (2005) *Phil. Trans. Royal Soc.* **363**, 509; Kumar, P., Franzese, G., Buldyrev, S. V., and Stanley, H. E. (2006) *Phys. Rev. E* **73**, 041505
29. Kumar, P., Franzese, G., and Stanley, H. E. (2008) *Phys. Rev. Lett.* **100**, 105701

30. Franzese, G., and Stanley, H. E. (2002) *J. Phys. Cond. Matter* **14**, 2201 (2002); *Physica A* **314**, 508
31. Stokely, K., Mazza, M. G., Stanley, H. E., and Franzese, G. (2008) arXiv: 0805.3468v3
32. Kumar, P., Franzese, G., and Stanley, H. E. (2008) *J. Phys.: Cond. Matt.* **20**, 244114
33. Pendas, A. M., Blanco, M. A., and Francisco, E. (2006) *J. Chem. Phys.* **125**, 184112
34. Isaacs, E. D., Shukla, A., Platzman, P. M., Hamann, D. R., Barbiellini, B., and Tulk, C. A. (2000) *J. Phys. Chem. Solids* **61**, 403
35. Ricci, M. A., Bruni, F., Giuliani, A. (2009) Similarities between confined and supercooled water, to appear on *Faraday Discussion*, in press
36. Ohno, K., Okimura, M., Akai, N., and Katsumoto, Y. (2005) *Phys. Chem. Chem. Phys.* **7**, 3005
37. Cruzan, J. D., Braly, L. B., Liu, K., Brown, M. G., Loeser, J. G., and Saykally, R. J. (1996) *Science* **271**, 59
38. Schmidt, D. A., and Miki, K. (2007) *J. Phys. Chem. A* **111**, 10119
39. Chaplin, M. (2007) "Water's Hydrogen Bond Strength", cond-mat/ 0706.1355
40. Franzese, G., and Stanley, H. E. (2007) *J. Phys.: Condens. Matter* **19**, 205126
41. Coniglio, A., and Peruggi, F. (1982) *J. Phys. A* **15**, 1873
42. Cataudella, V., Franzese, G., Nicodemi, M., Scala, A., and Coniglio, A. (1996) *Phys. Rev. E* **54**, 175; Franzese, G. (1996) *J. Phys. A* **29** 7367
43. Wolff, U. (1989) *Phys. Rev. Lett.* **62**, 361
44. The results of [41, 42] guarantee that the cluster algorithm described here satisfies the detailedbalance and is ergodic. Therefore, it is a valid Monte Carlo dynamics
45. Mazza M.G. et al. (2006) *Phys. Rev. Lett.* **96**, 057803; N. Giovambattista et al., (2004) *J. Phys. Chem. B* 1086655; M.G. Mazza et al. (2007) *Phys. Rev. E* **76**, 031203
46. Oleinikova, A., Brovchenko, I., (2006) *J. Phys.: Condens. Matter* **18**, S2247
47. We fit the boundary of the CPF scenario with the functional form $J_\sigma = a + bJ$, with $a = 0.30 \pm 0.01$ and $b = 0.36 \pm 0.01$
48. Maruyama, S., Wakabayashi, K., and Oguni, M. (2004) *AIP Conf. Proc. Proc.* **708**, 675
49. Oguni, M., Maruyama, S., Wakabayashi, K., and Nagoe, A. (2007) *Chem. Asian* 2, 514

50. Oguni, M., Kanke, Y., and Namba, S. (2008) *AIP Conference Proceedings* **982**, 34
51. Mazza, M. G., Stokely, K., Stanley, H. E., and Franzese, G. (2008) *arXiv:0810.4688*
52. Mallamace, F. (2008) preprint
53. Bruni, F. (2008) private communication
54 .*Our resolution in T does not allow us to observe the expected divergence of C_P upon approaching the critical poin*t.
55. Marques, M. I. (2007) *Phys. Rev. E* **76**, 021503
56. *The difference of our results with those in [55], i.e. the presence of two maxima also at $P < P_C$ and $T > T_C$ is due to the different choice of parameters for the model: here $J_\sigma < J < \varepsilon$ as in [13, 30, 31], while in [55] is $\varepsilon < J_\sigma < J$ which gives rise to a different phase diagram.*
57. *The non-zero value of C_P at low T is reminiscent of the appearance of the broad maximum. However the MF approximation is not able to reproduce the splitting of the maxima seen in MC at $P \gg P_C$*
58. *In the range of T of interest here the contribution to H of the UW term is negligible*